In Situ Investigation of Current Distribution in the Anode

Simon-Olivier Tremblay[1], Daniel Marceau[2], Duygu Kocaefe[3], Charles-Luc Lagacé[4], Marc Gagnon[5], François Laflamme[6] and Guy Ladouceur[7]

1. Ph.D student
2. Professor
3. Professor

1. University Research Centre on Aluminium (CURAL) - Aluminium Research Centre (REGAL) - University of Québec at Chicoutimi, Chicoutimi, Québec, Canada,
4. Continuous improvement and technology development
5. Technical Advisor
6. Supervisor technology development
7. Production Technician

2. Aluminerie Alouette Inc., Sept-Îles, Québec, Canada

Abstract

During the last few decades, there have been several improvements to the Hall-Héroult process to reduce the energy consumption. One of the modifications was the reduction of the anode-to-cathode distance (ACD), which increases the sensitivity of the cell. However, this can cause operational problems due to large variations of the current distribution in the electrolytic bath. To maintain operational stability while minimizing the ACD, a better understanding of the current distribution in the electrolytic bath is required. Considering the aggressive environment, an *in situ* current distribution in the bath remains difficult to obtain. In this paper, a new approach is proposed to allow correlations between the current distribution variations in a specific anode block and the change of surrounding *in situ* pot operational conditions such as alumina dissolution, bubble movement, metal pad deformation, etc. Since the current distribution on a specific horizontal plane in the anode block is linked to the evolution of the electrical resistance between the anode bottom and the cathode, the proposed approach could provide an efficient way to identify design and/or operational problems and take appropriate action.

Keywords: Current distribution in anode block; anode electrical resistance; in situ anode current distribution; in situ pot operational conditions.

1. Introduction

To improve aluminum production while minimizing the production cost, trends are moving towards greater cell amperage, larger anodes (to maintain acceptable current density) and lower anode-cathode distance (ACD). Those changes add further challenges to maintain a uniform current distribution in the cell.

Indeed, larger anodes and lower ACD lead to a low energy input and a small bath volume which can cause non-uniform alumina dissolution along the anodes, leading to a non-uniform current distribution. Also, the use of larger anode block lowers the current pickup rate which leads to a longer period of non-uniform current distribution [1]. Finally, with a lower ACD, the resistance between the anode bottom and the top of the metal pad (interpolar resistance) is reduced. This means that the resistance from the bubble movement and the metal pad distortion represent a higher percentage of the interpolar resistance than in case of large ACD. Then, considering the parallel circuit configuration, the uniformity of the current distribution across the anode panel becomes more sensitive to those local phenomena. The resulting non-uniform current distribution can lead to high magnetohydrodynamic (MHD) instability, thermal balance

disturbances and other operational problems such as anode spikes, perfluorocarbon (PFC) production and anode effects.

To improve the uniformity of the current distribution between anodes, the difference in electrical resistances of each electrical path (delimited by the anode stall location and the cathode) has to be minimal. Figure 1 shows the main features leading to variations of the electrical resistance between the anode stall and the cathode block.

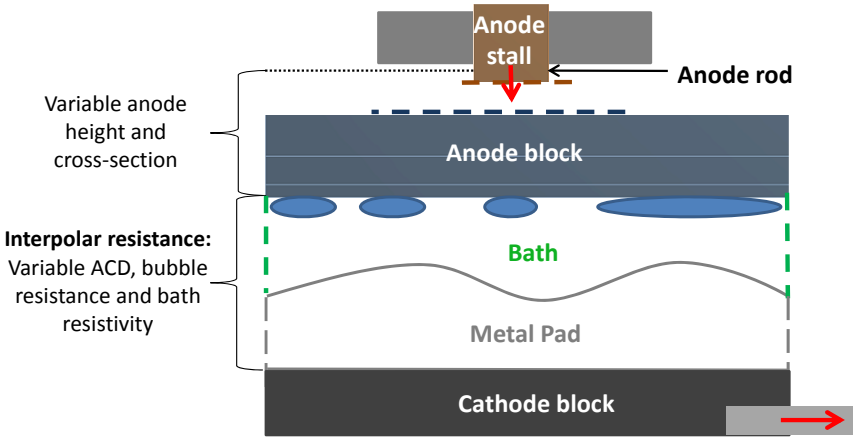

Figure 1. Elements leading to a variation of the electrical resistance.

Since the interpolar resistance variation is directly influenced by the surrounding pot operational conditions (alumina feeding, anode change, anode aging, anode effect, etc.), a better knowledge of the relationship between the *in situ* interpolar resistance variation and the surrounding pot operational conditions may lead to key elements for process optimization.

However, since each event, leading to an interpolar resistance variation, **can have a local impact under the anode bottom**, the anode rod current variation will give only the collective behavior of multiple events. In those cases, it may be difficult to correlate this information with pot operational conditions.

Therefore, **local measurements along the anode bottom would allow correlating the current distribution variation to a local variation of the interpolar resistance.** For instance, as bubble coverage locally increases the resistance and stops the electrolysis leading to higher current densities over the remaining anode bottom surface, the current distribution along the anode bottom would give valuable information about the local electrochemical process.

In this paper, since the current distribution in the anode block is linked to the interpolar resistance distribution (coming from variable ACD, bubble resistance and bath resistivity), an approach is proposed to allow correlating the current density distribution in a specific anode block with the change of *in situ* pot operational conditions.

2. In Situ Measurements

Considering the cell configuration, the aggressive environment and the fluctuations of the local electrical current, the *in situ* current distribution in an anode is difficult to measure.

As shown in Figure 2, the approach consists to use multiple voltage drops along the anode block to be able to interpret the current density distribution along the anode bottom.

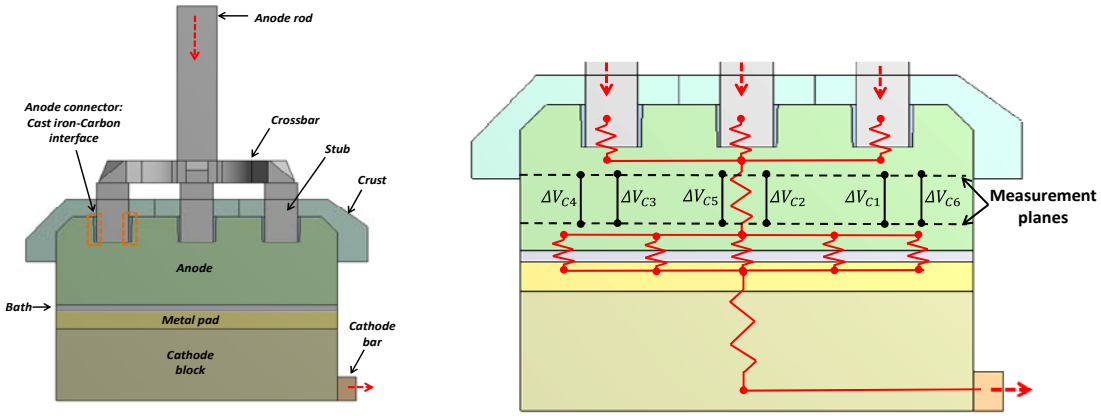

A) Model components

B) Electrical circuit representation with a projection of the voltage probes

Figure 2. Model components and electrical circuit representation.

To be able to get valuable voltage measurements, the height of the measurement planes have to be strategically determined. More specifically, the following conditions are required:

1) To be able to estimate accurately the resistance between the voltage probes in order to interpret the current density, see Equation (1). Therefore, to select a zone where the electric field lines are perpendicular to a known cross-section area.
2) To be in a zone where the current distribution reflects the interpolar resistance variation along the anode bottom;

$$I = \frac{\Delta V}{R} = \frac{\Delta V}{\left(\frac{\rho(T) L}{A_{Cross-section}} \right)} \quad (1)$$

where:

ΔV	Voltage difference between the two voltage probes, V
R	Resistance between the two voltage probes, Ω
$\rho(T)$	Material resistivity at a given temperature, Ωm
L	Length between the voltage probes, m
$A_{Cross-section}$	Cross section area perpendicular to the electric field lines, m^2

Considering the two conditions, it is necessary to analyze the anode current distribution evolution in response to an interpolar resistance change.

To do so, a mathematical model was built on ANSYS Workbench. The model process parameters, boundary conditions and resistance decomposition between the anode rod and cathode busbar are based on a previous measurement campaign [2].

The actual model is shown in Figure 3. The following input parameters and assumptions were used:

- Electrical resistivity and thermal conductivity of carbon, steel (yoke, stub, cathode collector bars) and cast iron (stub and cathode collector bar sealing) are taken from [3];
- Uniform electrical contact resistance of 0.25 $\mu\Omega m^2$ for each cast-iron to carbon interface (taken from [2]);
- A standard reversible electromotive force of -1.186 V at 970 °C is used [4];
- An anodic overvoltage of 0.8 V is used [5];
- An electrolytic bath conductivity of 212 S/m is used [6];

- The ACD was estimated using [2] results considering the previous assumptions;

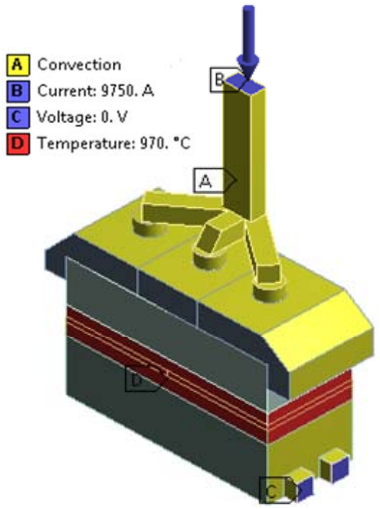

Figure 3. Boundary condition and model specifications.

The main objective of the simulations is to analyze the current distribution trends following a variation of the interpolar resistance distribution. Figure 4 and 5 show the current density distribution variation following a 50 % reduction of the interpolar resistance along 30 % of the anode bottom surface at the cell center side (left side). This event can take place following a neighboring anode change which can lead to a local metal pad distortion (local ACD reduction along the anode bottom surface).

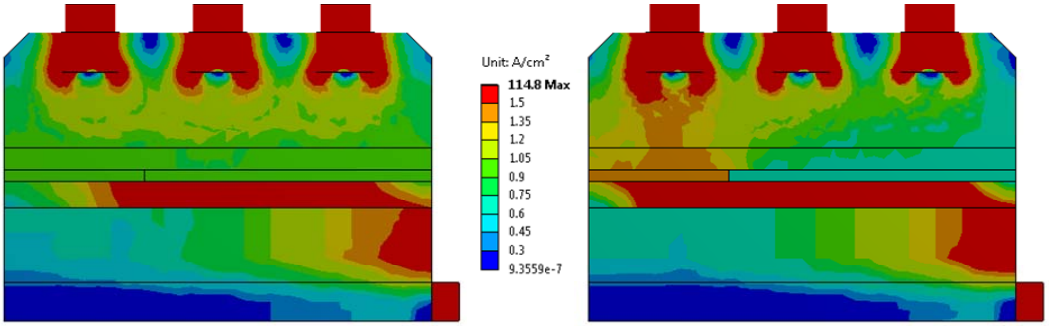

A) Uniform interpolar resistance B) Non-uniform interpolar resistance

Figure 4. Current density distribution in the anode as a function of interpolar resistance uniformity.

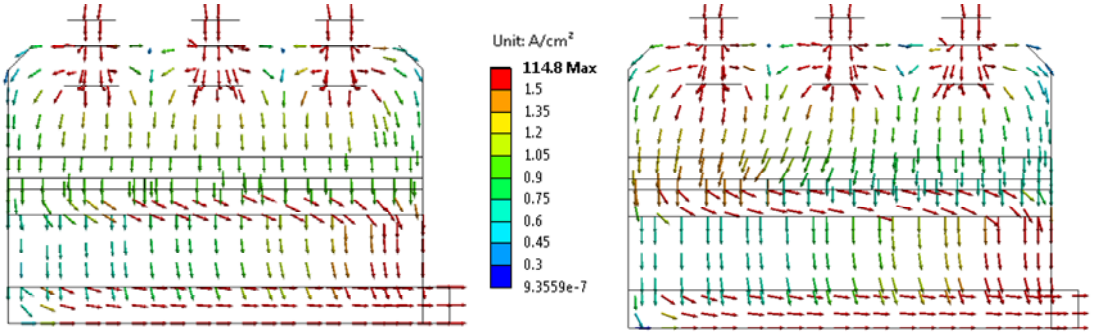

A) Uniform interpolar resistance B) Non-uniform interpolar resistance

Figure 5. Current density vectors in the anode as a function of interpolar resistance uniformity.

Figure 4 shows that the local reduction of the interpolar resistance has more influence on the current density distribution in the anode block than in the cathode block.

Indeed, since the current follows the less resistive path from the anode rod to the metal pad, the higher current density in the anode block will be reflected by the large interpolar resistance variation along the anode bottom.

On the other hand, the current distribution in the cathode block is not much influenced by the interpolar resistance variation (considering no sludge on the cathode surface). As shown by the higher current density and the associated vectors (Figure 4 and 5), to follow the less resistive path from the bath/metal interface to the cathode busbar, the current will travel along the highly conductive metal pad towards the shell (equalizing the non-uniform current distribution from the anode) to travel afterward a shorter path in the more resistive cathode bloc.

Also, Figure 4 B shows that the current density gets more sensitive to the interpolar resistance distribution closer to the anode bottom. Therefore, in order to detect smaller interpolar resistance variations, the measurement needs to be as close to the to the anode bottom as possible. However, the anodes being consumed, the measurement planes have to be placed higher up, but not too high either in order to avoid non-uniform current near the stubs. A reasonable compromise appeared to be to locate the measurement planes at around 200 mm and 300 mm from the anode top surface.

Considering the available equipment, 2 anode assemblies (4 anode blocks) were instrumented with 12 voltage probes per anode block (6 voltage measurement positions distributed on 2 measurement planes). Twelve rods made of stainless steel where inserted in each carbon block for voltage measurements. Figure 6 shows the instrumented anode.

Figure 6. Instrumented anode blocks.

In the anode block, the rods were laterally electrically insulated from the carbon, but the tips were in contact with the carbon. Voltage drop and temperature measurements were also made on each leg of the yoke to measure the current passing through each stub. The stub current distribution is taken into account for current density interpretation from the measurements in the anode blocks. The data acquisition interval was 0.2 s during the first 8 days and 5 s afterward.

Figure 7 shows the the spatial distribution of the probes and the nomenclature used in the experiment.

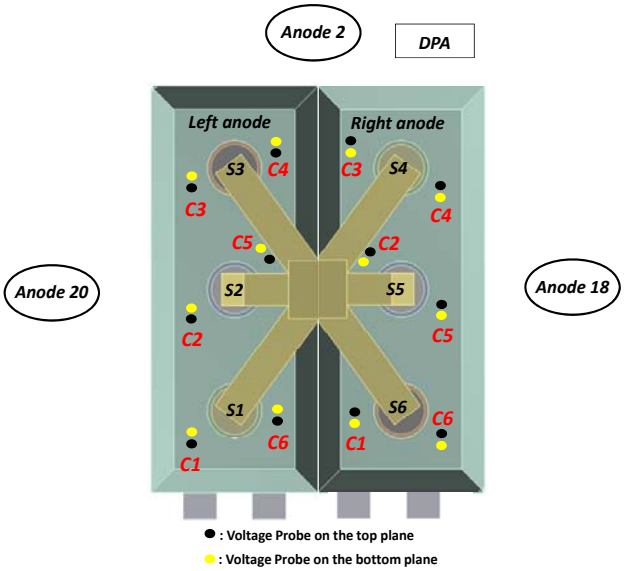

Figure 7. Representation of the instrumented anode assembly and nomenclature.

Since the voltage probes are not distributed uniformly in the anode, the area in Equation (1) is variable and this has to be taken into account in the calculation of the current densities from the voltage measurements.

3. Data processing

Using Equation (2), an application was developed on Maple which uses integration by finite elements in order to determine the current distribution in the anode from the acquired voltage measurements.

$$I_i = \int \mathbf{j}_i \bullet \mathbf{dA}_i \qquad (2)$$

where: $\mathbf{j_i}$ Current density vector, A/m^2
$\mathbf{dA_i}$ Differential arbitrary area vector, m^2
$\bullet$ Scalar product.

The application includes the following steps:

Reading of the in situ data:

- Voltage drops from the anode block (6);
- Specific localization of each voltage probe on the measurement plane (x, y);
- Distance between each associated voltage probe (z);
- Dimension of the measurement plane/anode cross section area (x, y);
- Resistivity of the anode carbon in function of temperature;
- Estimated temperature of the carbon between the two measurement planes;
- Total current passing through the anode (I measured).

Data construction for integration by finite elements:

- Definition of the number of integration points;
- Dimensioning and solving of the coordinate vectors and associated weight;
- Construction of the 2D (x, y, weight) scheme;
- Solving of the Jacobian function;

- Solving of the real coordinates and arbitrary area of integration points;
- Solving of the arbitrary area function for each integration point, A(x, y);

Data processing:

- Construction of the approximated function of the current density j(x, y): linear in y direction and quadratic in x direction (2 X 3 voltage measurements);
- Definition and initialization of the data matrix (x, y, j);
- Construction of the solution matrix for each integration point which includes:
  - Current density j(x, y),
  - Current I(x, y)
  - Interpolation error on current density,
  - Ratio between calculated current summation of I_i (I calculated) and the measured current from the yoke (I measured).

Considering the input parameters, the j(x, y) function can then be plotted for each time step in order to find correlations between the current distribution variations and the change of surroundings *in situ* pot operational conditions.

4. Preliminary Results

The following sections show the processed results for different associated pot operational conditions. Additionally, the stub current distribution and Fast Fourrier Transform (FFT) of the voltage probes will be used to provide a more reliable interpretation.

4.1. Current density quantification from voltage measurements

Since an adjacent anode change produces large current redistribution which can cause local metal pad distortions and lead to variation in the anode current density distribution, this specific event will be used to study the approach functionality. Figure 8 shows the measured anode current, 'I measured', the calculated anode current, 'I(x, y)', and the ratio 'I(x, y)'/'I measured' for a 160 s window taking place after 190 hours of operation.

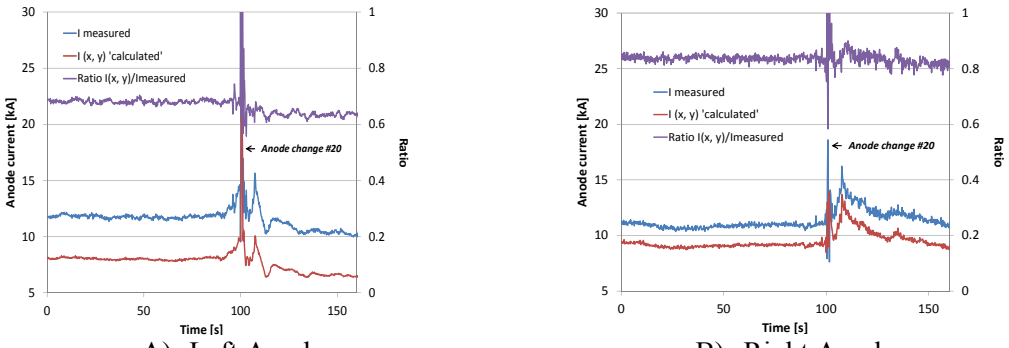

A) Left Anode B) Right Anode

Figure 8. Measured VS calculated anode current.

The lower calculated current 'I(x, y)' comes from the fact that the ratio of the distance between voltage measurements and the anode cross section is very small. Considering the nature of the carbon anode material, this leads to preferential electrical paths which underestimate the total anode current. A correction factor corresponding to the ratio 'I(x, y)'/'I measured' is used to obtain a more accurate quantification of the current densities. Note that the current pickup of the instrumented anodes was approximately 11 - 13 % larger than the average (during nearly the entire anode life) because they were set too low.

While in stable operation, the ratio 'I(x, y)'/'I measured' corresponds to approximately 0.68 for the left anode and 0.83 for the right anode. However, this ratio shows a greater variation when the anode current distribution becomes less uniform which induces higher current density gradients along the anode. Then, considering the limited number of measurements in the anode (2X3), the resulting approximated function of the current density (linear on the width and quadratic on the length) leads to larger extrapolation error with higher current density gradients.

To verify the functionality of the approach, Figure 9 shows the variation of the stub current during the anode change (at t = 101 s). For t = 39 s and t = 139 s, Figures 10 and 11 show snapshots of the calculated current density and the FFT of each measurement points with an observation time of 20 seconds (100 data at 0.2 s interval).

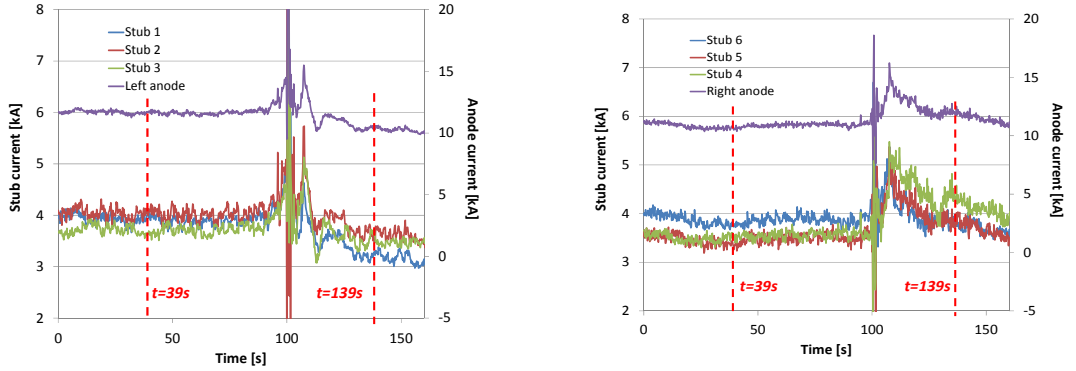

A) Left Anode B) Right Anode

Figure 9. Stub current distribution during an adjacent anode change.

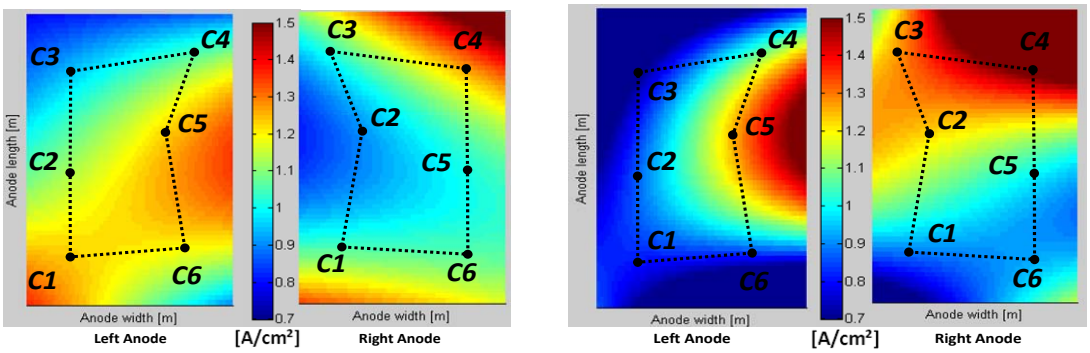

A) Before anode change, at t=39s B) Before anode change, at t=139s

Figure 10. Calculated current density distribution during an adjacent anode change.

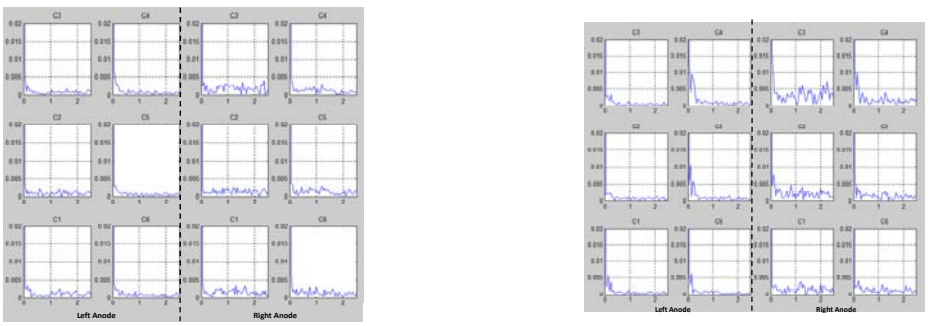

A) FFT at t = 39 s B) FFT at t = 139 s

Figure 11. FFT of measurements points during an adjacent anode change.

At t = 39 s (before the anode change), Figure 10 A shows that the anode current density is around 0.9 and 1.2 A/cm^2 which is in good agreement with the measured anode current and anode cross section. The lower current from stub 3 is well reflected by the smaller current density of the left anode at the cell centre side (C3-C4). Also, the lower current passing through stub 5 is well represented by the lower current density in the centre of the right anode (C2-C5). At t = 139 s (after the anode change), the stub current distribution (higher current in stub 2 and 4) is also well represented by the current density distribution in the left and right anode.

The FFT of Figure 11 B shows higher amplitude around 1 Hz for higher current density locations (C2-C3-C4) suggesting a higher sensitivity of the bubble movement due to a local decrease of the ACD in these regions.

However, even at stable operation, the current density can reach high values on the periphery of the anode due to extrapolation errors on j(x, y) because of the limited number of measurements along the section.

4.2. Effect of measurements proximity to the anode bottom

As previously discussed (section 2), the measurements need to be closer to the anode bottom in order to detect smaller variation of the interpolar resistance. As the anode is consumed, the measurements get closer to the anode bottom. Figure 12 compares the evolution of the anode current density measurements with the evolution of the stub current. Note that from 50 to 400 hours, the distance between the bottom measurement plane and the anode bottom goes approximately from 310 mm to 30 mm.

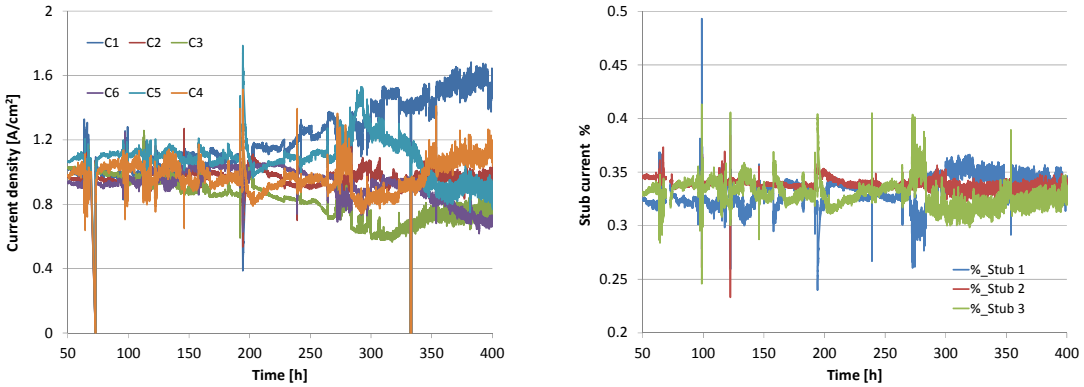

A) Anode current density (left anode) B) Stub current distribution (left anode)

Figure 12. Evolution of stub current and anode current density measurements.

For a same anode, Figure 13 A shows that the difference between the 6 carbon measurements gets larger as they get closer to the anode bottom. However, the difference between the stubs current stays in the same kind of order. These trends suggest that, as the anode is consumed, the current density measurements get more sensitive to the interpolar resistance variation. But, a higher sensitivity leads to a higher extrapolation error of the current density.

Figure 13 shows the resulting anode current density at t = 388 h. Indeed, the high current density gradients around measurements lead to large extrapolation error on the current density function which is amplified as the carbon is consumed.

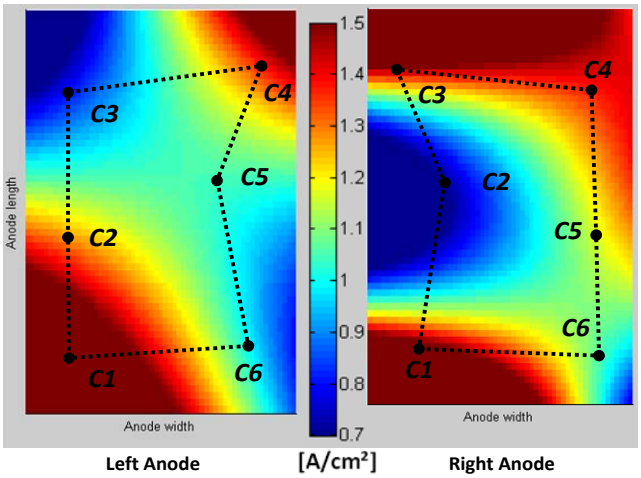

Figure 13. Current density gradient at measurements location.

5. Conclusions

- The approximated function of the anode current density, j(x, y), taken from the anode measurements is able to detect variation of the interpolar resistance distribution;
- The ratio between the calculated current summation according to Equation (2) and the measured anode current allows a better approximation of the resistance between the measurement planes which leads to a more reliable quantification of the anode current densities;
- Higher current density gradient along the measurements leads to larger extrapolation errors of j(x, y).
- A greater number of voltage probes along the measurement planes are needed to get a more accurate (higher polynomial degree) approximated function of j(x, y).

6. Acknowledgments

The authors acknowledge the financial support of the Fonds québécois de la recherche sur la nature et les technologies trough the Aluminum Center – REGAL, Nature Sciences and Engineering Research Council of Canada (NSERC) and particularly our industrial partners Aluminerie Alouette Inc.

7. References

1. A. Jassim, S. Akhmetov, B. J. Welch, M. Skyllas-Kazacos, J. Bao and Y. Yao, Studies on Background PFC emission in Hall-Héroult reduction cells using online anode current signals, Presentation at *TMS Light Metals Conference*, FL, Orlando, 2015.
2. S. Tremblay, D. Marceau et al. In situ investigation of the behavior of anode assemblies, *Light Metals* 2016, 959-964.
3. S. Wilkening and J. Côté, Problem of the stub-anode connection, *Light Metals* 2007, 865-873.
4. M.W. Chase et al., *JANAF Thermochemical Data*, 3nd ed. Nat. Bureau of Standards, Washington, 1975.
5. Henrik Gudbrandsen, Nolan Richards, Sverre Rolseth and Jomar Thonstad. Field study of the anodic overvoltage in prebaked anode cells, *Light Metals* 2003, 323-327.
6. J. Hives, J. Thonstad, Å. Sterten, and P. Fellner, Electrical Conductivity of Molten Cryolite-Based Mixtures Obtained with a Tube-Type Cell Made of Pyrolytic Boron Nitride, *Light Metals* 1994, 187.